Primary sensorimotor cortex exhibits complex dependencies of spike-field coherence on neuronal firing rates, field power, and behavior

Arce-McShane FI*[1], Sessle BJ[2], Ross CF[1], Hatsopoulos NG[1,3]

[1]Department of Organismal Biology and Anatomy, University of Chicago, 1027 E 57th Street, Chicago, IL 60637

[2]Faculty of Dentistry, University of Toronto, 124 Edward Street, Toronto, Ontario M5G 1G6, CANADA

[3]Committees on Computational Neuroscience and Neurobiology, University of Chicago, 1027 E 57th Street, Chicago, IL 60637

Corresponding author:

Dr. Fritzie Arce-McShane

Department of Organismal Biology and Anatomy, University of Chicago

1027 East 57th Street

Chicago, IL 60637

Tel: 773-702-5594; Fax: 773-702-0037

email: fritziea@uchicago.edu

Running title: *Complex dependencies between spike-field coherence and firing rates*

Abstract

Spike-field coherence (SFC) is widely used to assess cortico-cortical interactions during sensorimotor behavioral tasks by measuring the consistency of the relative phases between the spike train of a neuron and the concurrent local field potentials (LFPs). Interpretations of SFC as a measure of functional connectivity are complicated by theoretical work suggesting that estimates of SFC depend on overall neuronal activity. We evaluated the dependence of SFC on neuronal firing rates, LFP power, and behavior in the primary motor (MIo) and primary somatosensory (SIo) areas of the orofacial sensorimotor cortex of monkeys (*Macaca mulatta*) during performance of a tongue-protrusion task. Although we occasionally observed monotonically increasing linear relationships between coherence and firing rate, we most often found highly complex, non-monotonic relationships in both SIo and MIo, and sometimes even found that coherence decreased with increasing firing rate. The lack of linear relationships was also true for both LFP power and tongue-protrusive force. Moreover, the ratio between maximal firing rate and the firing rate at peak coherence deviated significantly from unity, indicating that MIo and SIo neurons achieved maximal SFC at a submaximal level of spiking. Overall, these results point to complex relationships of SFC to firing rates, LFP power, and behavior during sensorimotor cortico-cortical interactions: coherence is a measure of functional connectivity whose magnitude is not a mere monotonic reflection of changes in firing rate, LFP power, or the relevantly controlled behavioral parameter.

Keywords: orofacial cortex, motor cortex, somatosensory cortex, tongue protrusion, force, LFP

New and Noteworthy

The concern that estimates of spike-field coherence depend on the firing rates of single neurons has influenced analytical methods employed by experimental studies investigating the functional interactions between cortical areas. Our study shows that the overwhelming majority of the estimated spike-field coherence exhibited complex relations with firing rates of neurons in the orofacial sensorimotor cortex. The lack of monotonic relations was also evident after testing the influence of LFP power and force on spike-field coherence.

Introduction

Effective communication between areas of the cerebral cortex is critical for carrying out the simplest activities of daily living. Synchronous activity between cortical areas has been implicated in neuronal communication (Singer 1999; Fries 2005, 2015; Womelsdorf et al. 2007; Merchant et al. 2014; Bastos et al. 2015), and has been widely quantified using spectral coherence analysis (Pesaran et al. 2002, 2008; Brovelli et al. 2004; Gregoriou et al. 2009; Witham et al. 2010; Zagha et al. 2013; Arce-McShane et al. 2014, 2016; Menzer et al. 2014; Stetson and Andersen 2014; Thorn and Graybiel 2014). Often such analysis involves measuring the consistency *across trials* of the relative phases between the spike train of a neuron recorded during a specific time-period in one cortical area and the concurrent local field potentials (LFPs) recorded in another cortical area, i.e. spike-field coherence (Mitra and Pesaran 1999; Jarvis and Mitra 2001; Pesaran et al. 2002, 2008; Bokil et al. 2006; Gregoriou et al. 2009). Theoretical work has suggested that these estimates of spike-field coherence (SFC) depend on the firing rates of neurons whose spiking approximates a weak-sense stationary, discrete-time point process (Lepage et al. 2011). The work of Lepage et al. (2011) prompted studies investigating functional connectivity by using SFC analyses to demonstrate that differences in SFC are not a consequence of differences in firing rates between the two cortical areas. Some approaches have been suggested to correct this confound, thereby revealing changes in functional connectivity that are not due to changes in firing rates (Gregoriou et al. 2009; Grasse and Moxon 2010; Vinck et al. 2012; Lepage et al. 2013; Aoi et al. 2015). Indeed, studies on SFC have shown that, by applying spike thinning corrective measures, the observed changes in SFC measures between cortical areas were not affected by firing rate modulation (Gregoriou et al. 2009; Jia et al. 2013; Koralek et al. 2013; Stetson and Andersen 2014).

Correcting for the dependence of SFC on the number of spikes poses a challenge and a dilemma because oftentimes SFC estimates are used to compare interactions between cortical areas whose neurons exhibit intrinsically different firing patterns (Witham and

Baker 2007; Witham et al. 2010; Mochizuki et al. 2016) or different timescales of intrinsic fluctuations in spiking activity (Murray et al. 2014). This is particularly important when investigating sensorimotor areas of the cortex since, for example, the firing regularity of pyramidal neurons in the rat motor cortex is different from that in the somatosensory cortex (Mochizuki et al. 2016). Moreover, somatosensory and prefrontal areas of the cortex also exhibit shorter and longer timescales of intrinsic fluctuations, respectively (Murray et al. 2014). In macaques, the magnitude of LFP oscillations were strongest in the somatosensory areas while the intrinsic tendency of neurons to rhythmic firing was most prevalent in the primary motor cortex (Witham and Baker 2007). Similarly, some aspects of behavioral performance may influence the estimation of SFC. Therefore, the goal of this study was to evaluate the influence of neuronal firing rates, LFP power, and behavior on SFC estimates (Jarvis and Mitra 2001) by using spiking activity and LFPs recorded simultaneously from microelectrode arrays implanted in the primary somatosensory (SIo) and primary motor (MIo) areas of the orofacial sensorimotor cortex of monkeys during performance of a tongue-protrusion task. We estimated the SFC (Fig. 1a) between MIo spikes and SIo LFPs (MSf) and also between SIo spikes and MIo LFPs (SMf). Here we show that although differences in firing rates may influence the magnitude of the estimated SFC in the orofacial sensorimotor cortex, they do not do so in a simple, monotonic manner. The lack of linear relationships was also true for both LFP power and tongue-protrusive force.

Materials and Methods

Subjects. All recordings were made from two adult male rhesus macaques (*Macaca mulatta*), B (10 kg) and Y (12 kg). All protocols were approved by the University of Chicago Animal Care and Use Committee and carried out in accordance with the US National Institutes of Health Guide for the Care and Use of Laboratory Animals.

Behavioral task. Each monkey was trained to protrude its tongue onto a force transducer and apply isometric force at the level cued by the target position. Only one target position

was presented in each recording session (i.e. dataset). Detailed description of the task has been provided previously (Arce et al. 2013; Arce-McShane et al. 2014, 2016). Briefly, the trial started with the appearance of a cursor that represented the amplitude of the tongue-protrusive force applied on the transducer. After a random period between 0.75 to 1.25 s from trial-start, the base target window appeared to cue the monkey to keep the cursor within the base target window by generating force between 1-15 g for a random hold period between 0.5 and 1 s. Upon successful hold at the base target, the force target window appeared, signaling the monkey to move the cursor into the force target window (50 g for days 1-3, 80 g for days 4-5). To achieve success, the monkey had to generate a required force within the allotted time (5 s). To indicate success, the force target window changed color and the monkey immediately received a juice reward. We set an inter-trial interval of 3 s. The behavioral program was written using Spike2 software (Cambridge Electronic Design, Cambridge, England). Force transducer (Revere Transducers, Mode 462-D3-2-10P1R, Tustin, CA) signals and the behavioral event logs and timestamps were recorded at 2 kHz and stored using a Power 1401 data acquisition system (Cambridge Electronic Design, Cambridge, England). User-designed pulse signals generated to mark behavioral events were sent to the neural data acquisition systems for offline synchronization of timestamps across the different data acquisition systems.

Electrophysiology. Under general anesthesia, each monkey was chronically implanted with two silicon-based arrays of 100 microelectrodes (BlackRock Microsystems, Salt Lake City, UT), one in MIo and one in SIo of the left hemisphere. Each microelectrode on the array was separated from its immediate neighbors by 400 µm and its length was 1.0 mm for all implanted arrays except for one array where the electrode length was 1.5 mm (MIo of monkey Y). Implantation sites were verified based on surface landmarks and exhibited evoked responses from the tongue and face following monopolar surface stimulation of MIo (50 Hz, 200 µs pulse duration, 2-5 mA) during the surgical procedure. Signals from both arrays were amplified with a gain of 5000, simultaneously recorded digitally (14-bit) with a sampling rate of 30 kHz and hardware-filtered between 0.3-7.5 kHz (Cerebus

acquisition systems, BlackRock Microsystems, Salt Lake City, UT). This was followed by digital band-pass filtering for spikes (0.25-7.5 kHz) and for LFPs (0.3-250 Hz). LFPs were then resampled at 1 kHz. Spike waveforms were stored and sorted offline using Offline Sorter (Plexon, Dallas, TX). Only single units (i.e., well-separated clusters and waveforms based on at least three feature spaces in 2D) were included in all the analysis. Spikes that violated the minimum interspike interval (1.7 ms) were removed. Data from array channels with no signal or with large amounts of 60 Hz line noise were excluded.

Data analysis. Datasets used in this study were the same ones used previously (*n*=10, five datasets, D1-D5, from each monkey) (Arce-McShane et al. 2016). Briefly, we used a long-term learning paradigm wherein the subjects were exposed to the same behavioral task over days until they achieved a success rate >75% consistently for 3 days. For each dataset, we estimated the SFC between MIo spikes and SIo LFPs (MSf) and also between SIo spikes and MIo LFPs (SMf). LFP recordings during the analyzed behavioral window (-1 s to 0.5 s relative to force onset) were not contaminated by muscle activity from the temporalis muscles since there were no rhythmic jaw movements, such as those observed during licking or chewing. Furthermore, it has been shown that jaw-closing muscles such as the temporalis muscle are not active during this task in the monkey (Moustafa et al. 1994). Moreover, spectral power was modulated differently across frequency bands (see Figs. S9-S10 in Arce-McShane et al, 2016), suggesting that we were recording LFP oscillatory activity rather than muscle activity from the temporalis muscle. SFC was analyzed using the multitapers method of the Chronux Toolbox (Mitra and Pesaran 1999; Bokil et al. 2006). Coherence, C_{xy}, is a frequency-domain representation of the cross-correlation between two signals, i.e. the raw (unsmoothed) spike trains of neuron *x* and the LFPs of channel *y*. It is calculated as the cross-spectrum, S_{xy}, normalized by the geometric mean of their autospectra, S_{xx}, S_{yy} , respectively, $C_{xy} = \frac{S_{xy}}{\sqrt{S_{xx}S_{yy}}}$, where C_{xy} is a complex number whose modulus corresponds to the amplitude of coherence (0-1) and the argument as the relative phase difference between the two signals. We used a 0.5-s sliding window with 0.01-s steps and applied a time-bandwidth product, TW=3, and

orthogonal Slepian tapers, K=5, to the first 100 trials of the same task conditions. We have shown previously that the results of the theta SFC were comparable to coherence estimates using a 1-s window (see Supplementary Figure S3 in ref. 15). Here, we limit most analyses to the theta band (2-6 Hz) wherein larger and stronger sensorimotor networks were exhibited compared to other frequency bands (Arce-McShane et al. 2016). To determine the statistical significance of the modulation of theta frequency coherence, we calculated the coherence between paired signals by shuffling the trials (1000 repetitions) on one of the signals for the time window of the peak coherence (Arce-McShane et al. 2016). The shuffling procedure measures the coincident effects of motor output and sensory input and any residual coherence above the distribution of shuffles cannot be attributed to synchronization of motor output and sensory input. Paired signals with peak coherence that exceeded the highest 49th coherence amplitude obtained from shuffling were deemed to have significant modulation of coherence (p<0.05) and were the only ones used in all subsequent analyses (number of paired signals with significant modulation of spike-field theta coherence pooled across 5 datasets per monkey, Y: n_{MSf}=7741; n_{SMf}=9063, B: n_{MSf}=3170; n_{SMf}=2816). The results of the shuffling test was further verified by a cross-validation approach (see Supplementary Results in ref. 15). All subsequent analyses were performed on each dataset, unless specified otherwise. To evaluate linear dependence of SFC on mean firing rates, we performed a linear regression on the coherence magnitudes of many MIo neurons and a single LFP from one electrode in the SIo array (MSf) versus the mean firing rates of these MIo neurons using data obtained from the first 100 trials from a single recording session. We performed the same analysis for many SIo neurons and a single MIo LFP (SMf) versus the mean firing rates of these SIo neurons of the same dataset. These analyses were performed for each dataset (i.e. recording session) separately (Table 1). An F-test was performed to assess the significance of the regression slope at p<0.01 and at an adjusted p value after a Bonferroni correction for multiple tests. To verify that the results were not limited to inter-areal SFCs, we analyzed intra-areal SFC, i.e., between MIo neurons and MIo LFPs (MMf), and between SIo neurons and SIo LFPs (MMf). To verify that the results were not limited to inter-areal

SFCs in the theta band, we analyzed inter-areal SFCs in other frequency bands, i.e., alpha (6-13 Hz), beta (15-30 Hz), and gamma (30-50 Hz).

Using all successful behavioral trials in each dataset (Table 2), we also computed the SFC of each paired signal by categorizing behavioral trials based on firing rates, LFP power, or tongue-protrusive force and computing coherence for each grouping. Mean firing rates of a neuron during -0.3 to 0.2 s relative to force onset were sorted in ascending order prior to dividing the total number of trials into 10 groupings to yield firing rate categories of increasing magnitude. We then performed a linear regression of the coherence estimated from each grouping against the mean firing rate of that grouping. The same procedure was done for trial categories based on LFP power and force. We performed this analysis per dataset for each paired signal in MSf, SMf, MMf, and SSf (Table 2). The error of the estimates of the SFC for a smaller number of trials was not a concern here because each category had equal number of trials. More importantly, the dependence on rate relates to the fundamental aspect of the SFC measure. All other analyses were performed using built-in and user-defined functions in Matlab (Mathworks, Inc.).

Results

Consistent with previous studies, neurons in MIo and SIo modulated their firing rates (Fig. 1b) as the monkeys generated a tongue-protrusive force at the level of the cued target position (Murray and Sessle 1992; Lin and Sessle 1994; Arce-McShane et al. 2014, 2016). Likewise, LFPs in the theta frequency range (2-6 Hz) in MIo and SIo exhibited modulation of spectral power relative to the onset of the tongue-protrusive force (Fig. 1c). Spike-field coherence in both MSf and SMf was prominent in the theta band and was task-modulated, i.e. exhibiting increases and decreases relative to force onset. Figure 1d illustrates an example of MSf coherence between the spiking activity of a MIo neuron and an LFP signal recorded from a single electrode in SIo. A similar pattern of coherent activity was found between the spiking activity of a SIo neuron and an LFP signal recorded from a single electrode in MIo (Fig. 1d, SMf). As previously shown (see Supporting Information in

Arce-McShane et al, 2016), coherence exhibited modulation in other frequency ranges (6-13 Hz, 15-30 Hz, and 30-50 Hz) with peak coherence occurring at different times from -1.5 s to 1 s relative to force onset (i.e. time-evolved coherence was estimated using a 0.5-s sliding window with 0.01-s steps), indicating that the coherence was not simply reflecting an evoked potential and a spiking response to the onset of force. The mean theta coherence across the population of paired signals in MSf and in SMf showed an increase in coherence at ±0.2 s around force onset, albeit at different peak levels (Fig. 1e). We have reported previously that the theta coherence in MSf was significantly higher than the mean theta coherence in SMf (Arce-McShane et al. 2016). Examination of the mean firing rates at the time of peak coherence revealed that the firing rates of the population of MIo neurons were significantly higher than the firing rates of the population of SIo neurons in monkey Y (Empirical cumulative distribution function, $p<0.05$) but not in monkey B (Fig. 1f). Thus, the question arises whether the differences in SFC were a consequence of differences in firing rates between the two cortical areas, particularly in monkey Y. This question was the focus of the next phase of the analysis, as outlined below.

Relationship between firing rates of many different neurons and their SFC with the LFP signal from one electrode. To address the dependence of SFC on firing rates, we first examined whether SFC varied linearly with the mean firing rates of MIo and SIo neurons. To do this, we performed a linear regression of the firing rates of many single-units recorded on one microelectrode array on their coherence with the LFP signal recorded from a single channel on the other microelectrode array. This was done for each dataset separately. We used the mean firing rates and SFC values of the behavioral period corresponding to -0.3 to 0.2 s relative to force onset, during which we had observed a substantial difference between MSf and SMf. Figure 2a illustrates the result from an example of a regression test done in MSf; there were no significant linear (nor monotonic) relationship between the mean firing rates of many MIo neurons against their coherence with one LFP channel in SIo ($p>0.10$, *F*-Test on regression slope). Likewise for SMf of the

same dataset, we found no significant linear relationship between the mean firing rates of SIo neurons and their coherence with one LFP channel in MIo (Fig. 2a, $p>0.10$, *F*-Test on regression slope). Across all 10 datasets analyzed separately, 98.5% (±0.8% SEM) of the LFP channels in MIo (SMf) and 98.1% (±1.3% SEM) in SIo (MSf) did not show any significant linear dependence of the SFC on the mean firing rates ($p>0.01$, *F*-Test on regression slope). Figures 2b-c illustrate this result for every single LFP channel where LFPs in SIo and MIo, respectively, were recorded on a single session for monkey Y. Across all electrodes, there were none in MSf or very few electrodes in SMf (5 out of 75 MIo LFP channels, $p<0.01$) that showed significant linear relationships between firing rates and SFC. Using an adjusted p value after Bonferroni correction for multiple tests, the percentage of non-significant linear regression between SFC and firing rates measured at -0.3 to 0.2 s relative to force onset was 99.9% (±0.1% SEM) of the LFP channels in MIo and 100% in SIo across all datasets. Similar results were obtained when using different behavioral time windows in which SFC was estimated (i.e. -1.0 s to -0.5 s, -0.5 s to 0.0 s and -0.4 to 0.1 s relative to FO). Note that the results were consistent even for estimates of SFC at -1.0 s to -0.5 s prior to force onset, when firing rates were relatively sustained and there were no large fluctuations in firing rates due to movement onset nor due to differences in tongue-protrusive force. Thus, the vast majority of the estimated SFC, per dataset, did not exhibit a significant linear (nor monotonic) relationship with firing rates. We further probed whether a linear relationship existed when using intra-areal SFCs, i.e. between MIo neurons and its LFPs (MMf) and between SIo neurons and its LFPs (SSf). Across all 10 datasets analyzed separately, 99.1% (±0.7% SEM) of the LFP channels in MIo (MMf) and 98.5% (±0.6% SEM) in SIo (SSf) did not show any significant linear (nor monotonic) dependence of SFC on the mean firing rates (Fig. 2a, MMf and SSf, $p>0.01$, *F*-Test on regression slope prior to correction for multiple comparisons). Thus, the lack of linear dependence of SFC on firing rates was observed for coherences within and across cortical areas. Because spiking could be tied to LFPs by different mechanisms in different frequency bands, we also tested the linear relations in the alpha (6-13 Hz), beta (15-30 Hz), and gamma (30-50 Hz) frequency bands to show that the lack of linear dependence

of SFC on rates was not a specific feature of theta oscillations. We found similar results across all other frequencies; the majority of the LFP channels did not show any significant linear (nor monotonic) dependence of SFC on the mean firing rates (Table 3, p>0.01, *F*-Test on regression slope prior to correction for multiple comparisons). Thus, the lack of linear dependence of SFC on firing rates was observed across all frequency bands tested here.

Ratio between maximal firing rate and the firing rate at peak coherence deviated from unity. If there was a simple, monotonically increasing relationship between mean firing rates and SFC, one would also expect the maximal firing rate to occur at peak coherence. Our results did not bear this prediction out. Figure 3a-b shows the scatter plot of the maximal mean firing rate of MIo or SIo neurons and their mean firing rate at the time of peak coherence. The slope of the linear regression fit to the data deviated significantly from unity (Table 4, *t*-Test, $p<0.05$), indicating that neurons recorded from SIo or MIo achieved maximal coherence with LFPs recorded from the other cortical area at a submaximal level of firing rate. This behavior was found consistently across all datasets in SIo and almost all datasets in MIo in both monkeys. This suggests that other factors (e.g. behavioral contexts, cognitive load, or attention) may contribute to enhancing cortico-cortical interactions without driving the neuron to fire maximally. Consistent with our findings, the largest cortico-muscular coherence has been observed in monkeys during periods of steady holding of hand position when spiking activity was low and not during periods when spiking activity was high (Baker et al. 1997).

Relationship between firing rates of one neuron and its SFC based on trials with similar firing rates. It is possible that the heterogeneity of the neurons that we examined obscured the monotonic relation between firing rates and SFC; for example, neurons exhibit different firing patterns or intrinsic timescales of fluctuations in their spiking activity (Shinomoto et al. 2003; Witham and Baker 2007; Murray et al. 2014; Mochizuki et al. 2016). To test this, we computed the SFC for trials in which the neuron had similar

firing rates. All successful trials during a single recording session were sorted according to the mean firing rate calculated at -0.3 to 0.2 s relative to force onset. The sorted trials were then divided into 10 groups of equal trial number. This method controlled for neuronal heterogeneity since coherence was estimated for the same neuron across trial groupings with varying mean firing rates. Across all 10 datasets analyzed separately, 94.9% (±1.2% SEM) of the paired signals in MSf did not show significant linear relationships between coherence and mean firing rate (Fig. 4a, $p>0.01$, *F*-Test on regression slope). Nevertheless, our analysis did reveal a minority of pairs that showed significant positive linear relationships ($p<0.01$, 4-11% in monkey Y and 1-5% in monkey B). Surprisingly, a few pairs exhibited a significant negative linear relationship between coherence and mean firing rate ($p<0.01$, 1% in both monkeys). Figure 4b shows representative scatter plots of the MSf coherence calculated for 10 levels of firing rates of MIo neurons that showed a non-significant linear relation, significant positive, or significant negative linear relation. Similar results were found in SMf for both monkeys (Fig. 4c-d); across all 10 datasets analyzed separately, 97.5% (±0.6% SEM) in SMf did not show significant linear relations between SFC and mean firing rate based on trials with similar firing rates ($p>0.01$, *F*-Test on regression slope). Analysis using intra-areal SFC also yielded similar results (MMf: 97.8±0.5% SEM, SSf: 95.7±1.3% SEM).

Relationship between LFP power and SFC. Covariations in LFP amplitudes have been shown to influence the estimation of coherence between LFP signals (Srinath and Ray 2014) but have not been characterized for SFC. We evaluated the influence of varying LFP power on SFC by categorizing the trials according to LFP power and estimated the SFC per category. Across all 10 datasets analyzed separately, a vast majority of paired signals in MSf (97.1±0.3% SEM) and SMf (97.5 ±0.3% SEM) did not show significant linear (nor monotonic) relations between coherence and mean LFP power (Fig. 5a-top row, 5b, $p>0.01$, *F*-Test on regression slope). We found similar results for intra-areal SFC (Fig. 5a-bottom row, MMf: 96.8±0.5% SEM; SSf: 97.6±0.2% SEM). Of the few paired signals that showed significant linear relations, most exhibited decreasing SFC with increase in LFP

power (Fig. 5a-b). Similar results have been found in EEG recordings in humans; cortico-muscular coherence measured during precision grip was only slightly reduced when EEG power was doubled upon administration of diazepam (Baker and Baker 2003).

Relationship between force and SFC. Lastly, we evaluated whether SFC's relation to spike rate may depend on the behavior of the subject. We thus estimated SFC using trials categorized according to the level of tongue-protrusive force generated by the monkey. Across all 10 datasets analyzed separately, most paired signals in MSf (98.5±0.4% SEM) and SMf (98.8 ±0.3% SEM) did not show significant linear relations between coherence and mean force (Fig. 5c-top row, 5d, p>0.01, *F*-Test on regression slope). We found similar results for intra-areal SFC in MIo (99.0±0.2% SEM) and in SIo (98.4±0.3% SEM) (Fig. 5c-bottom row). These results are consistent with previously reported findings of lack of correlation of changes in coherence with changes in tongue protrusion force, success rates, reaction or movement times (Arce-McShane et al. 2016).

Relation between multiplying factor and rate categories. According to the theoretical analysis of Lepage et al. (2011), the theoretical intensity field coherence is a rate-independent measure of the probability that a neuron spikes at a specific phase of the LFP oscillation. It relates to SFC as follows: $C_{ny}(f) = C_{\lambda y}(f)\left(1+\frac{\mu_\lambda + H(f)}{S_{\lambda\lambda}(f)}\right)^{\frac{1}{2}}$, where $C_{ny}(f)$ is the SFC calculated at -0.3 to 0.2 s relative to force onset, $C_{\lambda y}(f)$ is the intensity field coherence, and the components of the multiplying factor are μ_λ: the mean rate, $S_{\lambda\lambda}(f)$: the spectrum of the rate λ_t, and *H(f)*: the parameter influenced by the history-dependent spiking (which we set to 0). From the equation, with increasing spiking activity, $\frac{\mu_\lambda}{S_{\lambda\lambda}(f)}$ tends to 0 and SFC equals the intensity field coherence. To test how the SFC relates with the intensity field coherence using empirical data, we estimated the multiplying factor for each rate category and tested its linear dependence on rate. We did not observe this linear dependence in most cases: in MSf, the value of the multiplying factor (~1.5) did not change linearly with increasing rates of MIo neurons for most paired signals (Fig. 6a);

only 8-16% of the paired signals exhibited a significant positive linear relation and 3-5% exhibited a significant negative linear relation with the different rate categories (p<0.01, F-Test on regression slope). Similarly in SMf, the value of the multiplying factor (~1.5) did not change linearly with increasing rates of SIo neurons for most paired signals; however, we found a higher percentage of negative linear relationships between the multiplying factor and the rate categories (16-32%) and a lower percentage of positive linear relationships (2-6%) compared to MSf (Fig. 6b). The difference in the proportion of negative relationships can be observed in the mean multiplying factor exhibiting a positive trend in MSf with increasing rate category, but a negative trend in SMf (Fig. 7a-b). The mean percentage difference between the mean multiplying factors for the lowest and highest firing rates across all datasets is 2.6% (±0.8% SEM) for MSf and -1.7% (±0.6% SEM) for SMf (Fig. 7a-b). The effect of different rates is considerably smaller than the mean percentage difference between the lowest and highest SFCs observed in our datasets (MSf: 26.9% (±2.9% SEM); SMf: 19.4% (±6.4% SEM), Fig. 7c-d, see also Fig. 1e). We found very few instances when SFC approximated the estimated intensity field coherence (compare Fig. 7c vs 7e and 7d vs 7f); that is, the value of the multiplying factor was 1(±0.05) in 4.7%(±0.5 SEM across datasets) instances in MSf and 13.0%(±0.4 SEM across datasets) in SMf. Contrary to their model prediction that the multiplying factor would be approximately 1 for firing rates exceeding some nominal value (Lepage et al. 2011), the mean firing rates associated with these values of the multiplying factor ranged from 3-57 spikes/s and median of 16 spikes/s in MSf and 2-52 spikes/s and median of 10 spikes/s in SMf (Fig. 8). These results do not support a monotonic increase in SFC with firing rates and suggest that our spiking data may not fit a weak-sense stationary, discrete-time point process model.

Discussion

The concern that estimates of SFC depend on the mean firing rates of single neurons (Lepage et al. 2011) has influenced analytical methods employed by experimental studies

investigating the functional interactions between cortical areas (Koralek et al. 2013; Dotson et al. 2014; Menzer et al. 2014; Stetson and Andersen 2014; Ray 2015). While Lepage et al (2011) demonstrated such dependence analytically, and in simulation of single neurons whose spiking approximates a weak-sense stationary, discrete-time point process, the dependence has not been tested using actual experimental recordings from many single-units. There have been efforts to develop analytical methods to address this possible confound of firing rate differences when interpreting observed differences in the amplitudes of SFC. Indeed, correction methods that adjust the firing rates of neurons when estimating the SFC have been suggested and applied to experimental data (Gregoriou et al. 2009; Jia et al. 2013; Aoi et al. 2015). Other studies suggested methods to reduce the bias of firing rates (Grasse and Moxon 2010; Vinck et al. 2012), however these methods study spike-field associations differently from the method used by Lepage et al (2011) and therefore are not considered here. We advocate instead an examination of the relation of firing rates and SFC as shown here before relying on corrective procedures that alter the observed firing rates of neurons in different cortical areas. Removing the possible confound of different firing rates may mask important properties of cortico-cortical interactions.

Comparing the properties of SFC between single-unit and multi-unit activity, Zeitler et al (2006) showed that the SFC was larger in multi-unit recordings than in single-unit recordings made from monkey visual cortex even though the number of spikes in both signals was comparable (Zeitler et al. 2006). Their experimental results were consistent with their model simulations relating a decrease in coherence with the square root of the mean firing rate and a linear increase in coherence with the modulation depth, thus supporting the proposition of Lepage et al (2011). In our study, we evaluated the dependencies between inter-areal SFC and neuronal firing rates of many single neurons in MIo and SIo measured experimentally. The results depicted in Figure 1 of Lepage et al. (2011) suggest that the dependence of SFC on firing rate can be approximated as linear in the limited range of coherence magnitudes that we have observed experimentally (0.04

393 to 0.4). Here, we showed that the vast majority of the estimated inter-areal and intra-
394 areal SFC, per dataset, did not exhibit a significant linear (nor monotonic) relationship
395 with firing rates. We have shown this both when comparing across multiple neurons with
396 varying firing rates (see Fig. 2) as well as when comparing a single neuron's firing rates
397 across similar behavioral trials (see Fig. 4). Both analyses yielded results that indicated
398 complex dependencies of SFC on the neurons' firing rates that were not captured by a
399 linear model. Such complexity may be attributed to factors such as variations in rate and
400 variability due to the randomness of spiking, non-Poissonian history effects, cellular or
401 synaptic dynamics, or neuronal morphology. More importantly, the two signals used to
402 estimate the SFC come from cortical areas that have been shown to exhibit different firing
403 properties and magnitudes of LFP oscillations (Witham and Baker 2007; Mochizuki et al.
404 2016). We also found a few cases in which the SFC decreased with increasing firing rates,
405 a surprising finding that may be explained by the fact that our experimentally-derived
406 multiplying factor (based on Equation 3.1 in Lepage et al., 2011) can decrease with
407 increasing firing rate (see Fig. 6). We found this negative relationship between firing rates
408 and SFC to be more prominent in SIo and may reflect an inhibitory mechanism to silence
409 irrelevant stimuli. A similar negative relationship has been reported in the macaque V1
410 when selective attention induced an increase in multi-unit spiking but a decrease in the
411 gamma SFC (Chalk et al. 2010).

412 Behavioral events can also induce changes in firing rates without a concomitant effect on
413 gamma synchronization in the visual cortex (Jia et al. 2013; Fries 2015). Here, we showed
414 that most relations between SFC and tongue-protrusive force were not monotonic (see
415 Fig. 5c-d), that is, increases in force did not vary linearly with SFC. This suggests that SFC
416 does not directly relate to the encoding of specific behavioral parameters and suggests a
417 role for coherence in spatiotemporal coordination of different functional networks that
418 emerge or are reshaped during learning (Arce-McShane et al. 2016). Lastly, the absence
419 of a linear relation between SFC and LFP power (see Fig. 5a-b) was consistent with our
420 previous findings that the modulation of LFP power did not follow the modulation of SFC

(Arce-McShane et al. 2016). This suggests that LFP oscillations and coherence may represent distinct functional roles (Baker and Baker 2003; Witham and Baker 2007).

In conclusion, the theoretical dependence of SFC on firing rates was not exhibited by our experimental data, suggesting that the theoretical dependence only holds under some assumptions and/or under some conditions. One possible reason is that our actual experimental data do not fit the weak-sense stationary, discrete-time point process model used by Lepage et al (2011) to describe this dependence. Indeed, the Fano factors of MIo and SIo neurons in our data were above 1 (see Fig. 10 in Arce-McShane et al., 2014), indicating that these neurons did not fit a Poisson model. Another possibility is that the SFC was derived using signals from cortical areas that exhibit intrinsically different timescales and firing patterns. Moreover, other factors such as synaptic mechanisms, circuit organization, or interneuron-pyramidal interactions may contribute to the absence of a linear behavior. Regardless, our findings point to complex relations between SFC and firing rates, LFP power, or force when examining sensorimotor cortico-cortical interactions during the performance of a behavioral task. The lack of linear or monotonic relations suggests that coherence is an appropriate measure of functional connectivity whose magnitude is not a mere monotonic reflection of changes in firing rate, LFP power, or the relevantly controlled behavioral parameter. Development of mathematical models to capture these complex relations is a direction for future work. Meanwhile, we advocate examination of the relation of firing rates and SFC as shown here before relying on corrective procedures that remove the bias of firing rates.

444 **References**

445 **Aoi MC**, **Lepage KQ**, **Kramer M a**, **Eden UT**. Rate-adjusted spike-LFP coherence
446 comparisons from spike-train statistics. *J Neurosci Methods* 240: 141–53, 2015.

447 **Arce-McShane FI**, **Hatsopoulos NG**, **Lee J-C**, **Ross CF**, **Sessle BJ**. Modulation dynamics in
448 the orofacial sensorimotor cortex during motor skill acquisition. *J Neurosci* 34: 5985–
449 5997, 2014.

450 **Arce-McShane FI**, **Ross CF**, **Takahashi K**, **Sessle BJ**, **Hatsopoulos NG**. Primary motor and
451 sensory cortical areas communicate via spatiotemporally coordinated networks at
452 multiple frequencies. *Proc Natl Acad Sci USA* 113: 5083–5088, 2016.

453 **Arce FI**, **Lee JC**, **Ross CF**, **Sessle BJ**, **Hatsopoulos NG**. Directional information from
454 neuronal ensembles in the primate orofacial sensorimotor cortex. *J Neurophysiol* 110:
455 1357–1369, 2013.

456 **Baker MR**, **Baker SN**. The effect of diazepam on motor cortical oscillations and
457 corticomuscular coherence studied in man. *J Physiol* 546: 931–942, 2003.

458 **Baker SN**, **Olivier E**, **Lemon RN**. Coherent oscillations in monkey motor cortex and hand
459 muscle EMG show task-dependent modulation. *JPhysiolLond* 501: 225–241, 1997.

460 **Bastos AM**, **Vezoli J**, **Fries P**. Communication through coherence with inter-areal delays.
461 *Curr Opin Neurobiol* 31: 173–180, 2015.

462 **Bokil HS**, **Pesaran B**, **Andersen RA**, **Mitra PP**. A method for detection and classification
463 of events in neural activity. *IEEE Trans Biomed Eng* 53: 1678–1687, 2006.

464 **Brovelli A**, **Ding M**, **Ledberg A**, **Chen Y**, **Nakamura R**, **Bressler SL**. Beta oscillations in a
465 large-scale sensorimotor cortical network: directional influences revealed by Granger
466 causality. *Proc Natl Acad Sci U S A* 101: 9849–54, 2004.

467 **Chalk M**, **Herrero JL**, **Gieselmann MA**, **Delicato LS**, **Gotthardt S**, **Thiele A**. Attention

reduces stimulus-driven gamma frequency oscillations and spike field coherence in V1. *Neuron* 66: 114–125, 2010.

Dotson NM, **Salazar RF**, **Gray CM**. Frontoparietal correlation dynamics reveal interplay between integration and segregation during visual working memory. *J Neurosci* 34: 13600–13, 2014.

Fries P. A mechanism for cognitive dynamics: neuronal communication through neuronal coherence. *Trends Cogn Sci* 9: 474–480, 2005.

Fries P. Rhythms for cognition: Communication through coherence. *Neuron* 88: 220–235, 2015.

Grasse DW, **Moxon KA**. Correcting the bias of spike field coherence estimators due to a finite number of spikes. *J Neurophysiol* 104: 548 LP-558, 2010.

Gregoriou GG, **Gotts SJ**, **Zhou H**, **Desimone R**. High-frequency, long-range coupling between prefrontal and visual cortex during attention. *Science* 324: 1207–10, 2009.

Jarvis MR, **Mitra PP**. Sampling properties of the spectrum and coherency of sequences of action potentials. *Neural Comput* 13: 717–749, 2001.

Jia X, **Tanabe S**, **Kohn A**. Gamma and the coordination of spiking activity in early visual cortex. *Neuron* 77: 762–774, 2013.

Koralek A, **Costa R**, **Carmena J**. Temporally precise cell-specific coherence develops in corticostriatal networks during learning. *Neuron* 79: 865–872, 2013.

Lepage KQ, **Gregoriou GG**, **Kramer M a.**, **Aoi M**, **Gotts SJ**, **Eden UT**, **Desimone R**. A procedure for testing across-condition rhythmic spike-field association change. *J Neurosci Methods* 213: 43–62, 2013.

Lepage KQ, **Kramer M a**, **Eden UT**. The dependence of spike field coherence on expected intensity. *Neural Comput* 23: 2209–2241, 2011.

Lin LD, **Sessle BJ**. Functional properties of single neurons in the primate face primary somatosensory cortex. III. Modulation of responses to peripheral stimuli during trained orofacial motor behaviors. *J Neurophysiol* 71: 2401–2413, 1994.

Menzer DL, **Rao NG**, **Bondy A**, **Truccolo W**, **Donoghue JP**. Population interactions between parietal and primary motor cortices during reach. *J Neurophysiol* 112: 2959–2984, 2014.

Merchant H, **Crowe D**, **Fortes A**, **Georgopoulos A**. Cognitive modulation of local and callosal neural interactions in decision making. *Front Neurosci* 8: 245, 2014.

Mitra PP, **Pesaran B**. Analysis of dynamic brain imaging data. *Biophys J* 76: 691–708, 1999.

Mochizuki Y, **Onaga XT**, **Shimazaki XH**, **Shimokawa T**, **Tsubo Y**, **Kimura R**, **Saiki A**, **Sakai Y**, **Isomura Y**, **Fujisawa S**, **Shibata K**, **Hirai D**, **Furuta T**, **Kaneko T**, **Takahashi S**, **Nakazono XT**, **Ishino XS**, **Sakurai Y**, **Kitsukawa T**, **Lee JW**, **Lee XH**, **Jung MW**, **Babul C**, **Maldonado XPE**, **Takahashi XK**, **Arce-mcshane FI**, **Ross CF**, **Sessle BJ**, **Hatsopoulos NG**, **Brochier T**, **Riehle A**, **Chorley P**, **Gru S**, **Taira M**, **Tsutsui K**, **Ogawa T**, **Komatsu H**, **Koida K**, **Toyama K**. Similarity in neuronal firing regimes across mammalian species. *J Neurosci* 36: 5736–5747, 2016.

Moustafa EM, **Lin LD**, **Murray GM**, **Sessle BJ**. An electromyographic analysis of orofacial motor activities during trained tongue-protrusion and biting tasks in monkeys. *ArchOral Biol* 39: 955–965, 1994.

Murray GM, **Sessle BJ**. Functional properties of single neurons in the face primary motor cortex of the primate. II. Relations with trained orofacial motor behavior. *J Neurophysiol* 67: 759–774, 1992.

Murray JD, **Bernacchia A**, **Freedman DJ**, **Romo R**, **Wallis JD**, **Cai X**, **Padoa-Schioppa C**, **Pasternak T**, **Seo H**, **Lee D**, **Wang X-J**. A hierarchy of intrinsic timescales across primate cortex. *Nat Neurosci* 17: 1661–1663, 2014.

Pesaran B, **Nelson MJ**, **Andersen RA**. Free choice activates a decision circuit between frontal and parietal cortex. *Nature* 453: 406–409, 2008.

Pesaran B, **Pezaris JS**, **Sahani M**, **Mitra PP**, **Andersen RA**. Temporal structure in neuronal activity during working memory in macaque parietal cortex. *Nat Neurosci* 5: 805–811, 2002.

Ray S. Challenges in the quantification and interpretation of spike-LFP relationships. *Curr Opin Neurobiol* 31: 111–118, 2015.

Shinomoto S, **Shima K**, **Tanji J**. Differences in spiking patterns among cortical neurons. *Neural Comput* 15: 2823–2842, 2003.

Singer W. Neuronal synchrony: a versatile code for the definition of relations? *Neuron* 24: 25–49, 1999.

Srinath R, **Ray S**. Effect of amplitude correlations on coherence in the local field potential. *J Neurophysiol* 112: 741–751, 2014.

Stetson C, **Andersen RA**. The parietal reach region selectively anti-synchronizes with dorsal premotor cortex during planning. *J Neurosci* 34: 11948–58, 2014.

Thorn CA, **Graybiel AM**. Differential entrainment and learning-related dynamics of spike and local field potential activity in the sensorimotor and associative striatum. *J Neurosci* 34: 2845–59, 2014.

Vinck M, **Battaglia FP**, **Womelsdorf T**, **Pennartz C**. Improved measures of phase-coupling between spikes and the local field potential. *J Comput Neurosci* 33: 53–75, 2012.

Witham CL, **Baker SN**. Network oscillations and intrinsic spiking rhythmicity do not covary in monkey sensorimotor areas. *J Physiol* 580: 801–14, 2007.

Witham CL, **Wang M**, **Baker SN**. Corticomuscular coherence between motor cortex,

somatosensory areas and forearm muscles in the monkey. *Front SystNeurosci* 4: 38, 2010.

Womelsdorf T, **Schoffelen J**, **Oostenveld R**, **Singer W**, **Desimone R**, **Engel AK**, **Fries P**. Modulation of neuronal interactions through neuronal synchronization. *Science* 316: 1609–1613, 2007.

Zagha E, **Casale AE**, **Sachdev RNS**, **McGinley MJ**, **McCormick DA**. Motor cortex feedback influences sensory processing by modulating network state. *Neuron* 79: 567–78, 2013.

Zeitler M, **Fries P**, **Gielen S**. Assessing neuronal coherence with single-unit, multi-unit, and local field potentials. *Neural Comput* 18: 2256–2281, 2006.

Acknowledgements

We thank Dr. Jason Lee, Kevin Brown and Dr. Kate Murray for assistance with the experiments, Matt Best for helpful discussions, and the veterinary staff of the University of Chicago for animal care. This work was completed in part with resources provided by the University of Chicago Research Computing Center.

Grants

This work was supported by CIHR Grant MOP-4918 and NIH RO1DE023816.

Additional Information

Competing financial interests

N.G.H. serves as a consultant for BlackRock Microsystems, Inc.

Figure Legends

Figure 1. Modulation of SFC, firing rates and LFP power during task performance. (a), Schema of paired signals used in the inter-areal coherence analysis: paired MIo spikes and SIo LFPs (MSf), and paired SIo spikes and MIo LFPs (SMf). **(b)**, Mean firing rates of one MIo neuron and one SIo neuron shown for ±0.05 s relative to force onset (FO), calculated using a 0.5 s sliding window with 0.01 s steps per trial, then averaged across trials. Gray shades denote 1 SEM. **(c)**, Modulation of spectral power of LFPs in the theta band (2-6 Hz). Data from a single electrode in MIo and another single electrode in SIo. **(d)**, Modulation of inter-areal SFC (2-6 Hz) shown for a paired signal in MSf and another paired signal in SMf**. (e)**, Mean tongue-protrusive force, theta MSf and SMf coherence across the populations of paired signals which exhibited significant coherence (Shuffle test, $p<0.05$). Data from D5 of monkey Y (n_{MSf} = 2369 pairs, n_{SMf} = 2094 pairs) and D3 of monkey B (n_{MSf} = 419 pairs, n_{SMf} = 639 pairs). Shades denote 1 SEM. **(f),** Empirical cumulative distribution function (ECDF) and 95% lower and upper confidence bounds for the ECDF of the population rates of neurons in MIo (Y: n=91, B: n=57) and in SIo (Y: n=79, B: n=27) shown in (e). Data used mean firing rates corresponding to the period of 0.5 s prior to FO to FO (***left, gray shaded plot***) and from FO to 0.2 s after FO (***right, blue shaded plot***).

Figure 2. Relation between firing rates and SFC. (a), MSf, plot of relation between firing rates of many different MIo neurons to the coherence between these neurons and a single SIo LFP from one electrode (MSf). A dot represents the mean firing rate of one MIo neuron plotted against the magnitude of its coherence with a single SIo LFP. Mean firing rates and coherence were calculated for -0.3 s to 0.2 s relative to force onset. The other plots are as in MSf but for firing rates of many different SIo neurons against their coherence with a single MIo LFP (**SMf**), MIo neurons against their coherence with a single MIo LFP (**MMf**),SIo neurons against their coherence with a single SIo LFP (**SSf**). **(b),** In each subplot, the mean firing rates of many MI neurons are plotted against their theta MSf coherences with SIo LFP signal from one electrode. The placement of the subplot corresponds to the relative position of the electrode on the 10x10 array from which the

593 SIo LFP was recorded (i.e. 74 subplots correspond to 74 electrodes). Shown only for paired
594 signals that showed significant coherence (Shuffle test, $p<0.05$). For all subplots, mean
595 firing rates and coherence were calculated for -0.3 s to 0.2 s relative to FO and same x and
596 y axes were used. The linear fit of rates to coherence was not significant for any LFP
597 channels (*F*-test on regression slope, $p>0.01$). Data from D5 of monkey Y. Similar results
598 were obtained from other time windows, other days, and for monkey B. Reproduced from
599 Supplementary figure S13A in (Arce-McShane et al. 2016) **(c),** As in (b) but for firing rates
600 of many SIo neurons plotted against their theta SMf coherences with MIo LFP signal from
601 one electrode. Firing rates correspond to SIo neurons and the position of the subplot
602 corresponds to the electrode from which MIo LFP was recorded. Data from D5 of monkey
603 Y. For this dataset, there were 5 out of 75 electrodes that showed a significant linear fit
604 (*=$p<0.01$ *F*-test on regression slope, gray line).

605 **Figure 3. Ratio between maximal firing rate and the firing rate at peak coherence. (a),**
606 Each subplot shows the linear relation between maximal firing rate and the firing rate at
607 peak coherence for each dataset, D1 to D5. Shown for MIo neurons (upper row, n= [1082
608 1417 1414 1459 2369]) and SIo neurons (lower row, n= [1609 1940 2035 1385 2094]) of
609 monkey Y. Regression fit (solid gray line) significantly differed from the unity line (dashed
610 gray line) for most datasets (*=$p<0.05$ *t*-Test). Neurons included in the plot are all those
611 that showed significant coherence with LFPs (Shuffle test, $p<0.05$). **(b),** As in (a) for
612 monkey B (MIo: n= [735 846 419 662 508], SIo: n= [509 620 639 446 602]).

613 **Figure 4. SFC based on trials with similar firing rates. (a),** Proportion of paired signals that
614 showed nonsignificant, significant positive or negative linear relation between MIo firing
615 rates and MSf calculated based on trials with similar firing rates (*F*-Test on the regression
616 slope, $p<0.01$). Mean firing rates and coherence were estimated for -0.3 to 0.2 s relative
617 to FO. Shown for 2 sample datasets from each monkey. **(b),** Scatter plots of the MSf
618 coherence (y axis) calculated for 10 levels of firing rates (x axis) during the same time
619 window used in (a). Two examples of MIo neurons that showed nonsignificant (***upper***
620 ***row***), a positive (***middle row***), or a negative (***lower row***) linear relationship. Shown

separately for each monkey. **(c-d),** As in (a-b) for SIo firing rates and SMf calculated based on trials with similar firing rates.

Figure 5. SFC based on trials with similar LFP power or force. (a), Proportion of paired signals that showed non-significant linear relation and significant positive or negative relation between SFC and LFP power. Shown for each dataset and type of SFC. **(b),** Examples of paired signals in MSf that showed significant relation of SFC to LFP power. Data from D5 of monkey Y. **(c),** As in (a), but between SFC and tongue-protrusive force. Shown for each dataset and type of SFC. **(d),** Examples of paired signals in MSf and SMf that showed significant relation of SFC to LFP power. Data from D5 of monkey Y.

Figure 6. Multiplying factor and rate categories. (a), *Upper row,* Nine examples of the relationship between the multiplying factor and rate categories. Each subplot shows the value of the multiplying factor of the MSf coherence of a paired signal (Equation 3 (Lepage et al. 2011)) as a function of increasing firing rate categories of a MIo neuron. Multiplying factor was calculated based on our experimental data from monkey Y, Day 5. Asterisks denote significant positive or negative linear relationship between the multiplying factor and MIo rate categories. *Lower row,* Distributions of the slope of the linear regression between the multiplying factor in MSf and MIo rate categories for D1 to D5. Colors denote non-significant and significant positive or negative linear relationship. **(b),** As in (a) for multiplying factor in SMf against SIo rate categories.

Figure 7. Mean multiplying factor, coherence, and rate categories. (a-b), Mean multiplying factor as a function of increasing firing rate categories. Shown for MSf and SMf, respectively. Data from monkey Y, Day 5. **(c-d),** Mean SFC and **(e-f),** intensity (rate)-field coherence as a function of increasing firing rate categories. Intensity-field coherence was estimated using Equation 3 (Lepage et al. 2011). Shown for MSf and SMf, respectively. Data from monkey Y, Day 5.

Figure 8. Varying rates for values of the multiplying factor approximating 1. (a-b), Multiplying factor for values 0.95-1.05 and their corresponding mean firing rates. Shown

for MSf and SMf, respectively. Data, from monkey Y, pooled across all training days. **(c-d),** Distribution of mean firing rates of MIo neurons and SIo neurons shown in a-b, respectively.

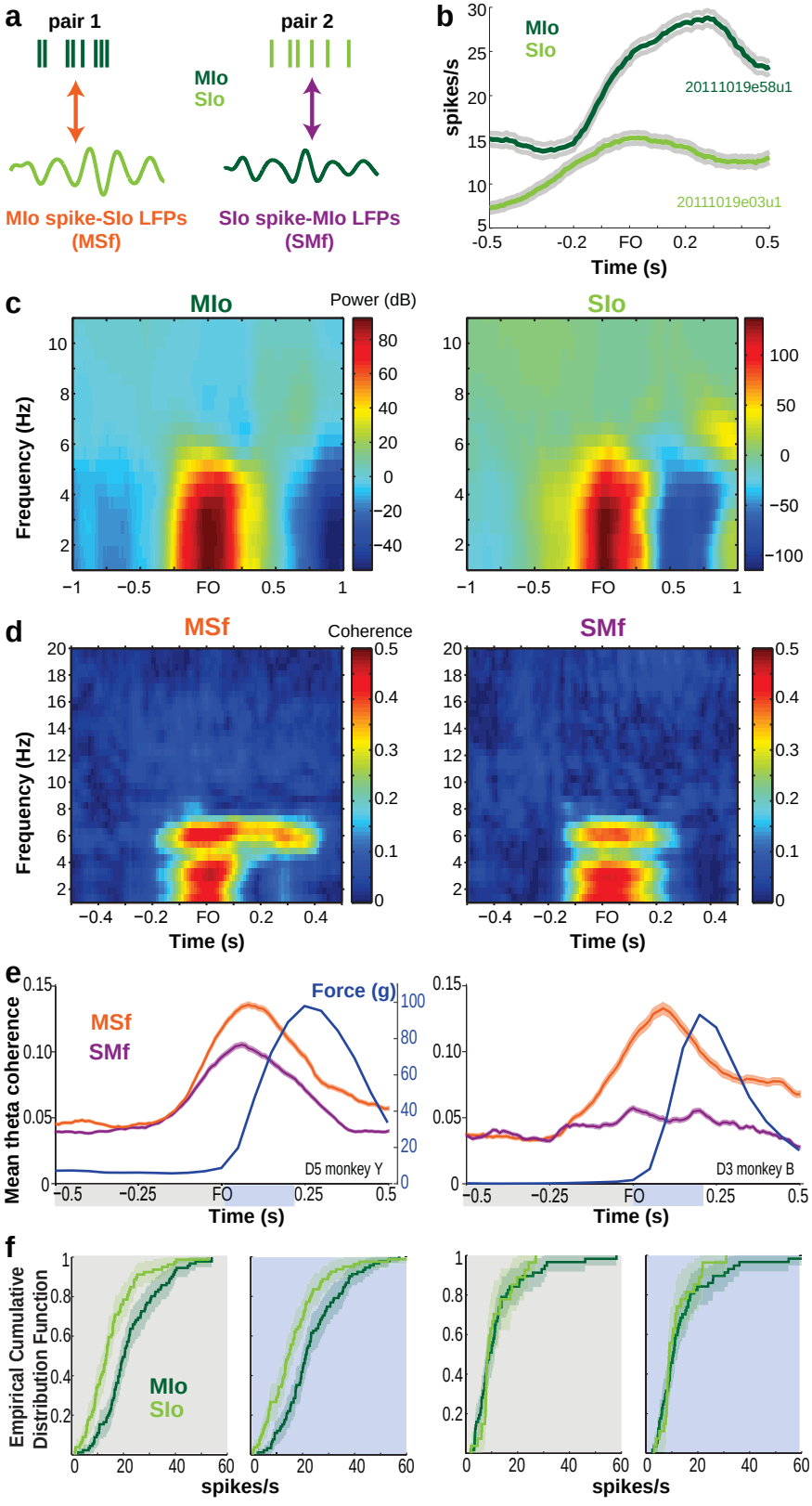

Figure 1

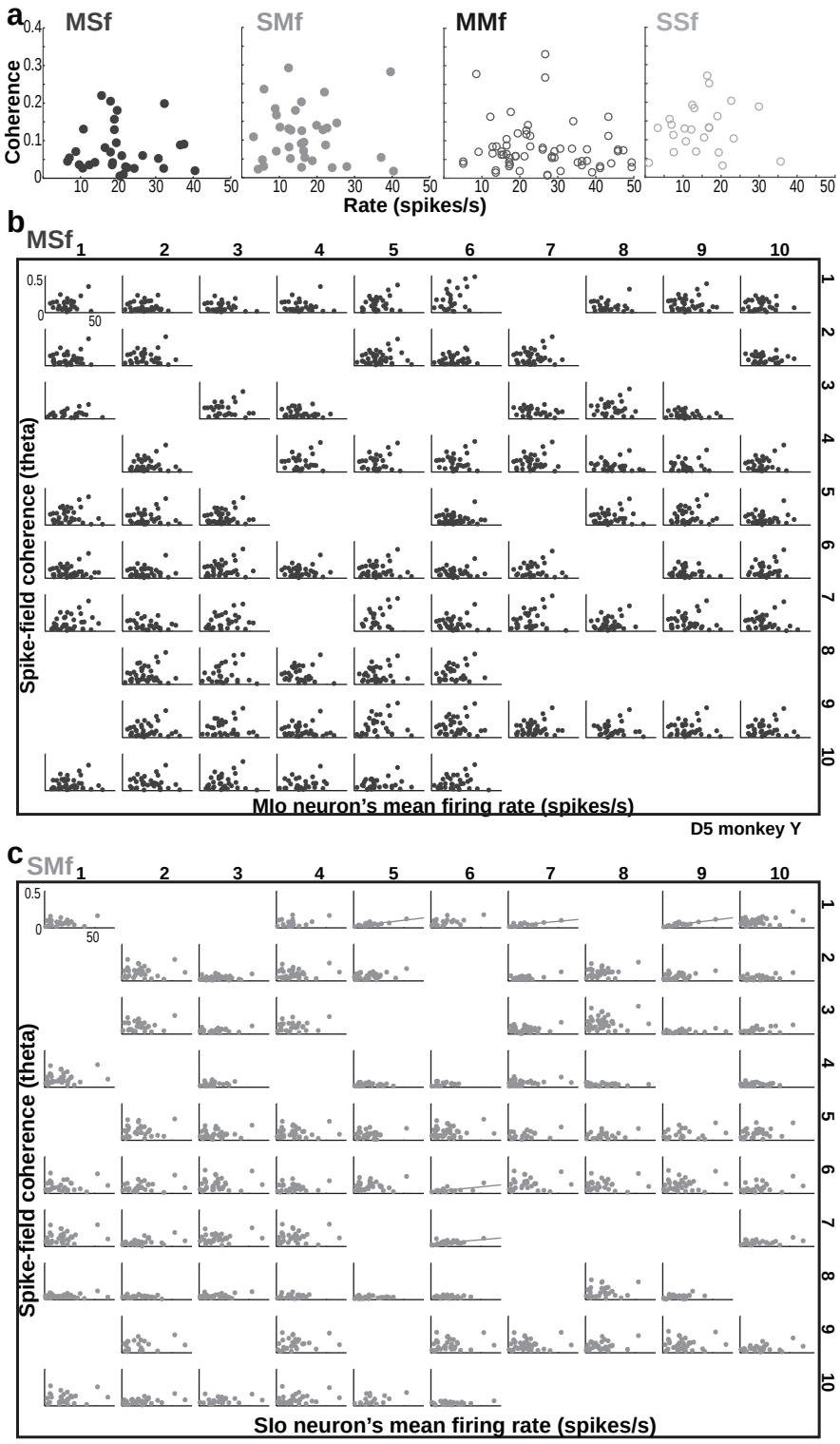

Figure 2

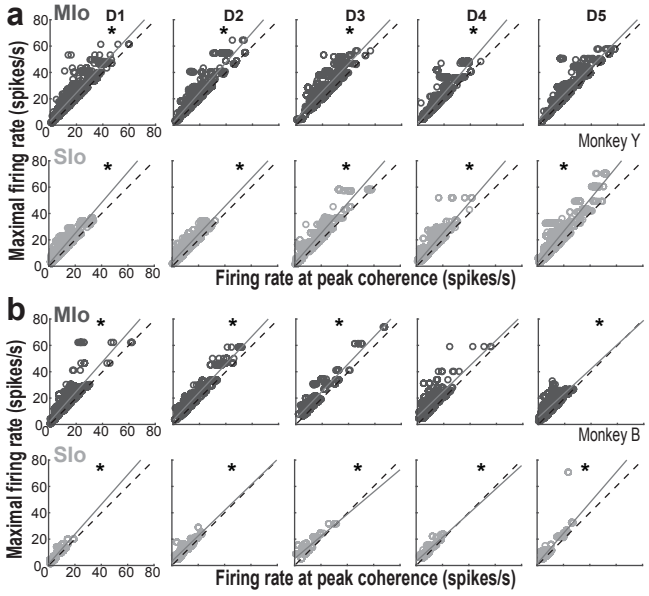

Figure 3

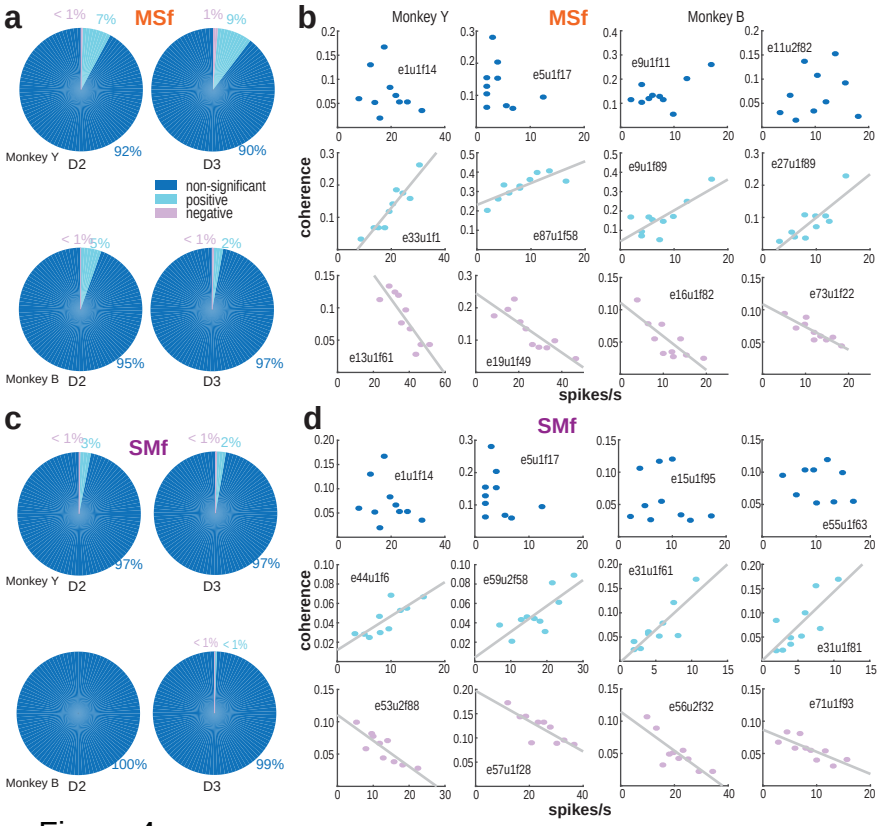

Figure 4

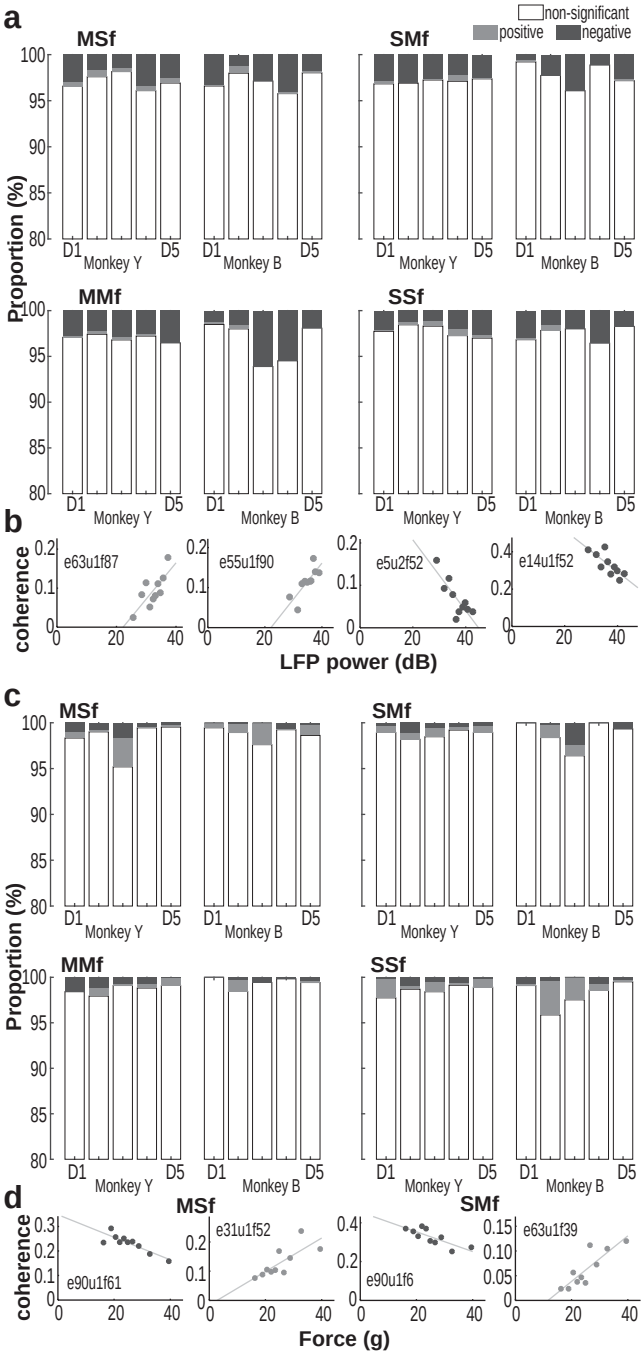

Figure 5

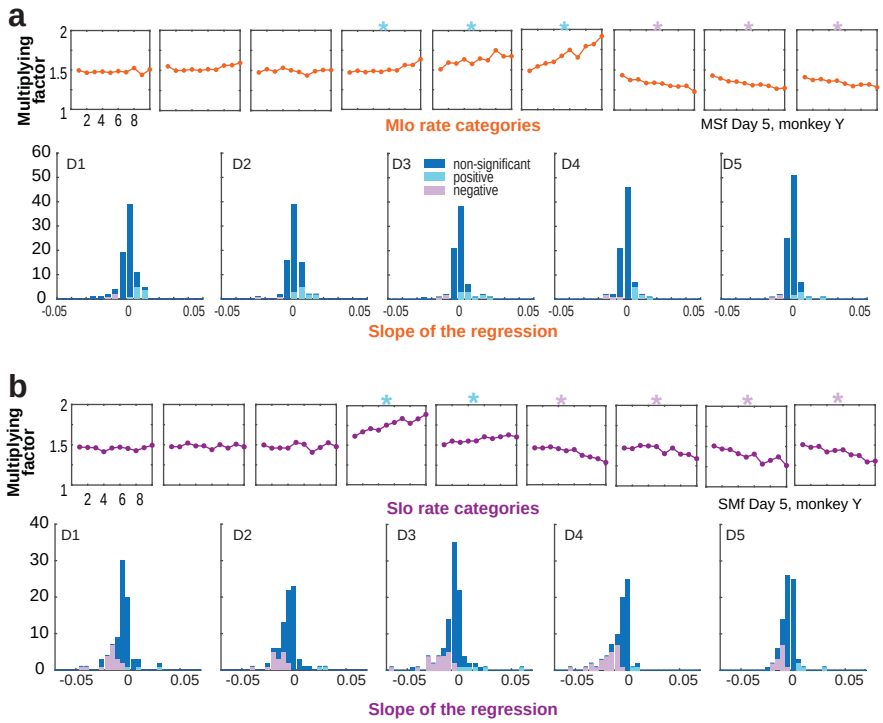

Figure 6

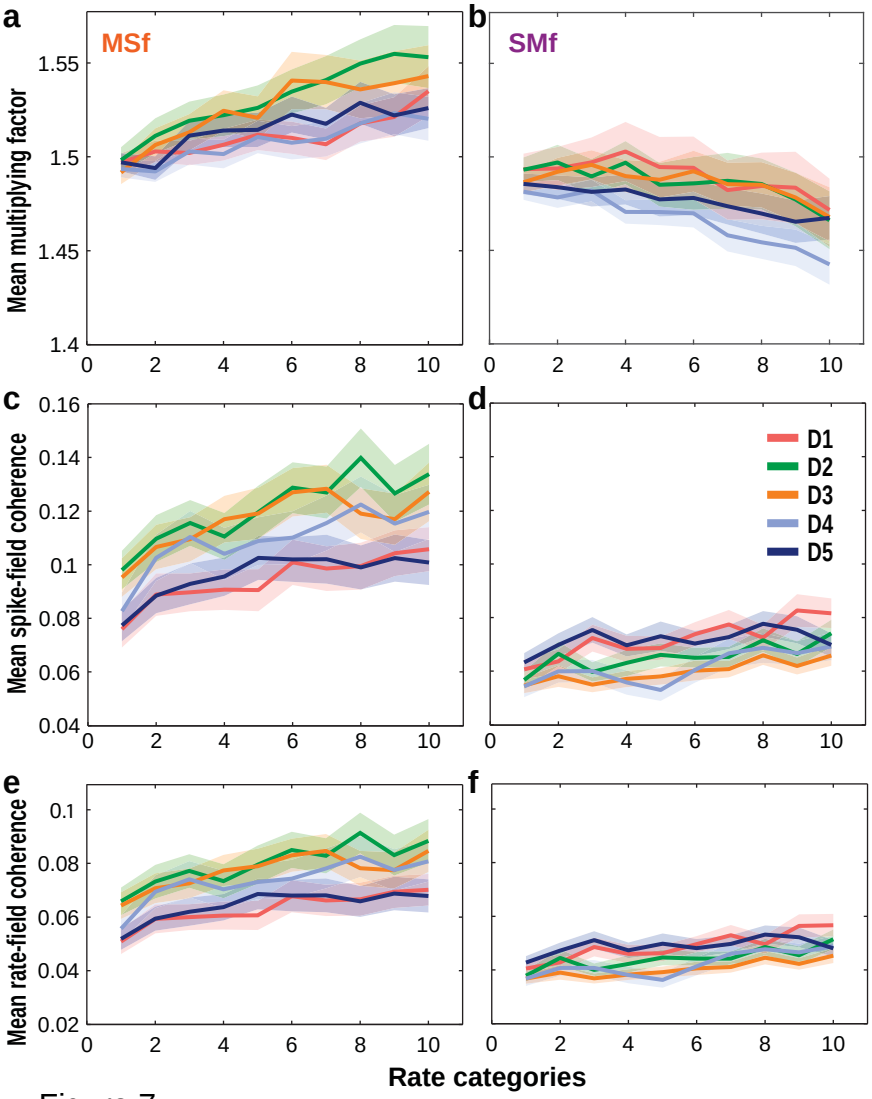

Figure 7

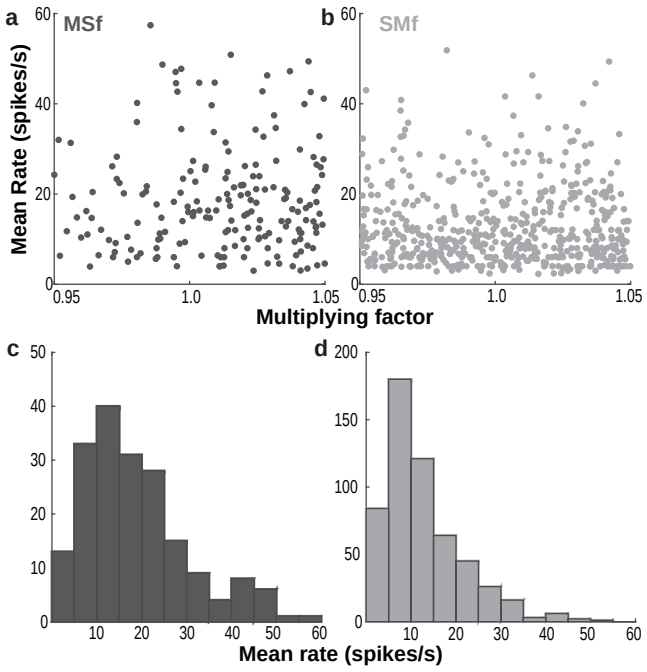

Figure 8

	MSf						SMf					
	Monkey Y			Monkey B			Monkey Y			Monkey B		
	Neurons per test	LFP channels	Unique neurons	Neurons per test	LFP channels	Unique neurons	Neurons per test	LFP channels	Unique neurons	Neurons per test	LFP channels	Unique neurons
D1	15(7-29)	72	82	24(18-33)	30	60	22(13-32)	72	85	10(4-19)	52	30
D2	19(11-30)	74	79	24(11-36)	35	59	32(21-48)	61	82	12(7-20)	53	36
D3	17(9-26)	84	76	17(9-23)	25	57	31(21-44)	65	102	13(9-17)	48	27
D4	21(11-32)	70	84	22(13-31)	30	56	22(12-36)	62	78	9(6-13)	47	33
D5	32(23-42)	74	91	15(8-23)	34	50	28(16-39)	75	79	15(9-19)	41	38

Table 1. Descriptive statistics for the regression tests. Shown per dataset (D1-D5) in MSf and SMf for each monkey (Y and B). Columns 1-2 per monkey correspond to the number of neurons (mean and range) and LFP channels used per regression test. Column 3 corresponds to the number of unique neurons per dataset.

	Trials		MSf		SMf		MMf		SSf	
	Monkey Y	**Monkey B**	**Monkey Y**	**Monkey B**	**Monkey Y**	**Monkey B**	**Monkey Y**	**Monkey B**	**Monkey Y**	**Monkey B**
D1	323	213	1082	735	1609	509	1268	928	1550	441
D2	287	255	1417	846	1940	620	1550	1155	1681	508
D3	352	254	1414	419	2035	639	143	884	2774	202
D4	420	146	1459	662	1385	446	1440	621	1721	281
D5	300	348	2369	508	2094	602	2135	522	2298	406

Table 2. Descriptive statistics for the regression tests based on trial categories. Column 1 corresponds to the total number of trials used in the regression test. Shown per dataset for each monkey. Columns 1-2 per monkey correspond to the number of neurons (mean and range) and LFP channels used per regression test. Column 3 corresponds to the number of unique neurons per dataset.

	MSf			SMf		
	Nonsignificant	Positive	Negative	Nonsignificant	Positive	Negative
Theta	98.1(1.3)	1.6(1.3)	0.3(0.3)	98.5(0.8)	1.0(0.8)	0.5(0.4)
Alpha	98.9(0.5)	0.8(0.4)	0.3(0.3)	99.4(0.4)	0.3(0.3)	0.3(0.3)
Beta	99.2(0.4)	0.5(0.2)	0.3(0.2)	98.9(0.9)	1.1(0.9)	0
Gamma	100	0	0	99.5(0.5)	0.2(0.2)	0.2(0.2)

Table 3. Proportion of paired signals (%) that showed nonsignificant, significant positive or negative linear relation between rates and SFC in different frequency bands. Values are mean and ±1 SEM across all 10 dataset.

MIo Y	**Estimate**	**SE**	**tStat**	**p Value**
D1 Intercept	3.1427	0.26674	11.782	3.1375e-30
slope	1.0725	0.014012	76.546	0
D2 Intercept	2.2842	0.26995	8.4615	6.4953e-17
slope	1.1355	0.013706	82.852	0
D3 Intercept	4.6728	0.35886	13.021	1.0946e-36
slope	1.0556	0.016346	64.575	0
D4 Intercept	1.0157	0.24394	4.1637	3.3149e-05
slope	1.1659	0.013145	88.692	0
D5 Intercept	4.008	0.1974	20.304	1.2745e-84
slope	1.0135	0.0081226	124.77	0
SIo Y				
D1 Intercept	1.7538	0.11468	15.293	2.1484e-49
slope	1.1615	0.01022	113.65	0
D2 Intercept	3.0811	0.13209	23.326	2.8547e-106
slope	1.0576	0.010108	104.63	0
D3 Intercept	2.4159	0.13853	17.439	1.3952e-63
slope	1.1356	0.0087651	129.56	0
D4 Intercept	1.8763	0.16532	11.349	1.3217e-28
slope	1.1551	0.013875	83.25	0
D5 Intercept	2.1116	0.19757	10.688	5.3811e-26
slope	1.2195	0.010309	118.3	0
MIo B				
D1 Intercept	2.2725	0.3099	7.3331	5.9654e-13
slope	1.133	0.021653	52.325	1.0229e-249
D2 Intercept	3.2678	0.19536	16.727	1.8483e-54
slope	1.0633	0.010438	101.86	0
D3 Intercept	4.2831	0.30746	13.931	1.7289e-36
slope	1.0493	0.015803	66.399	7.6838e-224
D4 Intercept	6.0607	0.3387	17.894	1.1272e-58
slope	0.96611	0.029197	33.089	2.7649e-142
D5 Intercept	5.3356	0.33679	15.842	3.3872e-46
slope	0.92113	0.031658	29.096	4.1296e-110
SIo B				
D1 Intercept	1.1723	0.1244	9.424	1.5388e-19
slope	1.1274	0.019728	57.146	4.1705e-223
D2 Intercept	3.1745	0.18879	16.815	1.5863e-52
slope	0.96592	0.016538	58.406	8.7336e-254
D3 Intercept	5.2149	0.27125	19.225	2.6421e-65
slope	0.84306	0.026443	31.882	4.6217e-134
D4 Intercept	3.1292	0.17816	17.564	8.072e-53
slope	0.90864	0.017864	50.865	2.5831e-187
D5 Intercept	1.2444	0.34736	3.5825	0.00036797
slope	1.1573	0.028343	40.833	2.3337e-175

Table 4. Linear regression between maximal firing rates and firing rates at peak coherence. Estimated coefficient values (intercept and slope) and their related statistics, shown for D1 to D5 of MIo and SIo of monkeys Y and B (***Estimate***). Standard error of the estimate (***SE***), *t*-statistic for each coefficient to test the hypothesis that the coefficient is equal to zero or not (***tStat***), p-value for the *F* statistic of the hypothesis that the coefficient is equal to zero or not (***p Value***).